



ChemComm

**Carbon content drives high temperature superconductivity
in a carbonaceous sulfur hydride below 100 GPa**

Journal:	<i>ChemComm</i>
Manuscript ID	CC-COM-06-2022-003170.R1
Article Type:	Communication

SCHOLARONE™
Manuscripts

Cite this: DOI: 00.0000/xxxxxxxxxx

Carbon content drives high temperature superconductivity in a carbonaceous sulfur hydride below 100 GPa

G. Alexander Smith,^{a,b} Ines E. Collings,^c Elliot Snider,^d Dean Smith,^a Sylvain Petitgirard,^e Jesse S. Smith,^f Melanie White,^{a,g} Elyse Jones,^d Paul Ellison,^g Keith V. Lawler,^a Ranga P. Dias,^{d,h} Ashkan Salamat,^{a,g,*}

Received Date

Accepted Date

DOI: 00.0000/xxxxxxxxxx

We report a previously unobserved superconducting state of the photosynthesized carbonaceous sulfur hydride (C-S-H) system with a maximum T_c of 191(1) K below 100 GPa. The properties of C-S-H are dependent on carbon content, and x-ray diffraction along with simulation reveals the system retains molecular-like packing up to 100 GPa.

The superhydride superconductor is envisioned as a hydrogen dominant alloy which lowers the pressure required to achieve the favorable properties and high- T_c predicted for dense metallic hydrogen.^{1–4} Hydrogen within these alloys takes part in an extended bonding network, be it the purely hydrogenic clathrate sublattice of a metal superhydride, or a covalent network with other elements as in H_3S .^{5–7} There have been record breaking milestones within the covalent superhydrides, including a 203 K T_c for H_3S at 155 GPa^{8–10} and a 288 K T_c at 267 GPa in carbonaceous sulfur hydride (C-S-H).¹¹ C-S-H was first synthesized from elemental precursors at 4 GPa, and then compressed without thermal annealing into its final reported superconducting state, a

pathway likely leading to metastable states. C-S-H has since been synthesised by reacting elemental S and CH_4-H_2 fluid mixtures.¹² In principle, this method permits greater control of C concentration, although the reported C–H Raman modes are comparably weak, and whether it leads to high- T_c states is yet to be studied. From either synthetic route, C-S-H displays a rich phase diagram below 100 GPa where evidence points to a retention of molecular-like packing as well as metallization.^{11,12}

While the exact identity of the record-breaking C-S-H material has yet to be discerned, candidate structures have been proposed from crystal structure prediction (CSP) and virtual crystal approximation simulations.^{13–18} Many of the CSP candidates for C-S-H are molecular or exhibit a molecular sub-unit, including the leading candidates with CH_4 intercalating or replacing an H_3S unit within the H_3S perovskite-like lattice.^{13,14,17,19} While these low-dimensional sub-units seem contrary to the extended bonding network, our recent simulations showed that dispersion interactions can potentially be important in covalent superhydrides with such sub-units.²⁰ Along these lines, it was recently discovered that a metal superhydride with a relatively low hydrogen concentration, YH_6 , exhibits an anomalously high T_c at lower pressures than its more studied higher hydrogen content counterparts.²¹

Building on the high T_c s reported at 100s of GPa for the superhydrides, the next goal towards achieving ambient superconductivity is to lower the critical pressure required to form superconducting phases.²² Herein, we investigate C-S-H below 100 GPa to probe for lower-pressure superconducting states predicted by CSP, and to further understand the consequences of the thermodynamic pathway for synthesizing C-S-H from elemental precursors. We present electrical transport measurements in this previously unexplored pressure regime that reveal a remarkably high T_c in some crystals, raising the question as to how these macroscopic quantum states emerge over such dramatically different P - T ranges. Synchrotron single crystal X-ray diffraction (SC-XRD) identifies structural evolution of C-S-H up to 100 GPa and Ra-

^a Nevada Extreme Conditions Laboratory, University of Nevada, Las Vegas, Las Vegas, Nevada 89154, USA

^b Department of Chemistry & Biochemistry, University of Nevada, Las Vegas, Las Vegas, Nevada 89154, USA

^c Centre for X-ray Analytics, Empa – Swiss Federal Laboratories for Materials Science and Technology, Überlandstrasse 129, 8600 Dübendorf, Switzerland

^d Department of Mechanical Engineering, University of Rochester, Rochester, New York 14627, USA

^e Department of Earth Sciences, ETH Zürich, Zürich 8025, Switzerland

^f HPCAT, X-ray Science Division, Argonne National Laboratory, Illinois 60439, USA

^g Department of Physics & Astronomy, University of Nevada, Las Vegas, Las Vegas, Nevada 89154, USA

^h Department of Physics & Astronomy, University of Rochester, Rochester, New York 14627, USA

* E-mail: ashkan.salamat@unlv.edu

† Electronic Supplementary Information (ESI) available: XRD details and results including refinements equations of state, reciprocal space reconstructions, and images; additional transport data; and simulations details and snapshots. See DOI: 00.0000/00000000.

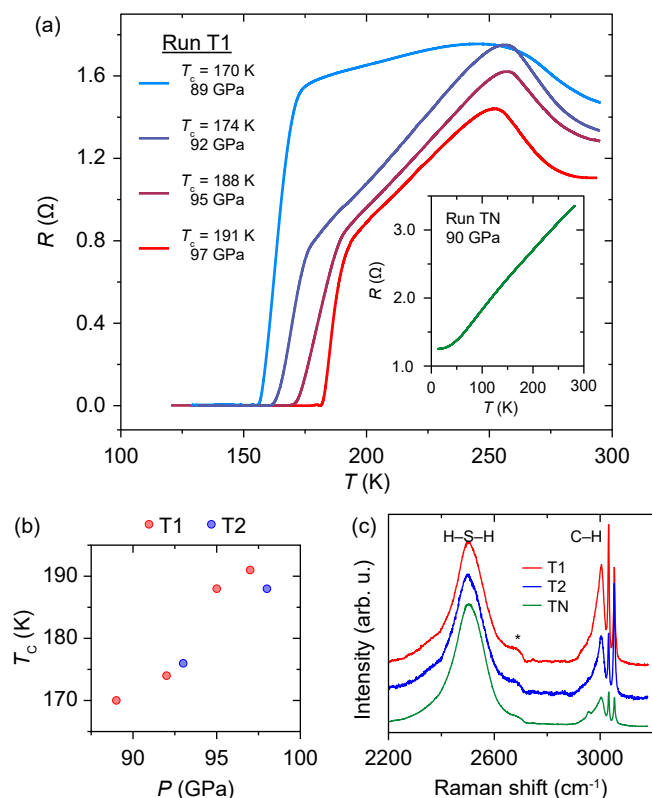


Fig. 1 (a) Resistance response of C-S-H (Run T1) on cooling, displaying a superconducting transition at 191 K at 97 GPa. (Inset) R response from Run TN at 90 GPa showing metallic behavior. (b) Evolution of T_c with P for Runs T1 and T2. (c) Comparative Raman spectra of Runs T1 and T2, and Run TN at 4.0 GPa and 300 K. The feature marked with an asterisk (*) is second-order Raman scattering from diamond.

man spectroscopy shows that the C content in C-S-H produced by photochemistry varies in each crystal synthesised. That variation directly affects the material properties with subtle differences in packing densities. Density functional theory (DFT) assists in understanding the H positions of the determined phases.

All crystals of C-S-H here are synthesized using the procedure of Snider *et al.*¹¹ (full details in ESI). Ball-milled mixtures of elemental C and S with dimensions about 15% of the diamond culet (typically 100–250 μm) are placed into the sample chamber of a diamond anvil cell, along with a ruby sphere.²³ Gas phase H_2 is loaded at 0.3 GPa.²⁴ Samples are then pressurized to 3.7–4.0 GPa and excited for several hours using light from a 514 nm laser with power ranging from 10 and 150 mW depending on sample response. Crystal growth is monitored *in situ* by visual observation, and Raman spectroscopy confirms the transformation into C-S-H by the presence of characteristic C-H, S-H, and H-H Raman modes. Samples are compressed to 10 GPa after transformation and characterization by Raman spectroscopy to avoid decomposition.

We performed electrical transport measurements on 3 newly-synthesized crystals of C-S-H – Runs T1, T2, and TN – following the methods described in Snider *et al.*¹¹ (Fig 1). In 2 separate runs, we observe maximum T_c s of 191(1) K at 97(5) GPa (Run T1, Fig 1a and Fig 1b) and 188(1) K at 98(5) GPa (Run T2, Fig 1b).

These transitions occur at roughly half the pressure required to achieve a similar T_c in either C-S-H or S-H/S-D.^{11,25} Runs T1 and T2 are contrasted with Run TN, which does not exhibit a superconducting transition at 90(5) GPa on cooling to 10(1) K, despite exhibiting metallic character (Fig 1a inset). The shape of the T_c vs. pressure (Fig 1b) implies this superconductivity comes from a distinct phase than that at 267 GPa. Also observed in Run T1 is the previously noted behavior of C-S-H to exhibit increasingly narrow $\Delta T/T_c$ as a function of increasing pressure and T_c , exhibiting a minimum $\Delta T/T_c$ of 0.0373 at 97 GPa (data in ESI).

By virtue of our focus on the lower pressure phases of the C-S-H ternary, the samples used in this study are significantly larger than those in Snider *et al.*¹¹, by a factor of 3–10, and these larger crystals have a heterogeneous C concentration compared with crystals from our previous work. This inhomogeneity is evidenced by variations in the relative intensities of Raman modes originating from C-H stretches around 3000 cm^{-1} and H-S-H bends around 2500 cm^{-1} , ie. $I_{\text{C-H}}/I_{\text{H-S-H}}$. Fig 1c shows representative Raman spectra of C-S-H crystals from each of the three runs following their initial synthesis at 4 GPa, with variations in $I_{\text{C-H}}/I_{\text{H-S-H}}$ evident. Run TN, which did not exhibit a superconducting transition at 90(5) GPa, has an intensity ratio $I_{\text{C-H}}/I_{\text{H-S-H}}$ of 0.27. Meanwhile, Runs T1 and T2 have $I_{\text{C-H}}/I_{\text{H-S-H}}$ of 1.16 and 0.93, respectively. It is important to note that even our Run TN has a higher $I_{\text{C-H}}/I_{\text{H-S-H}}$ than the samples reported in Snider *et al.*¹¹ which become superconducting at room temperature under compression ($I_{\text{C-H}}/I_{\text{H-S-H}} = 0.08$). Thus, increased C concentration in the C-S-H ternary system is linked to a significant reduction in the pressure required to reach the superconducting regime.

Each of the $R(T)$ responses at the different pressures measured from Run T1 feature a turning point above the superconducting transition around 250 K (Fig. 1a). At these conditions C-S-H exhibits the temperature response of a finite gap system, whereas just below 250 K the temperature response is metallic. This behavior at 250 K likely results from either a structural or electronic phase transition. An electronic transition would not likely be accompanied by a change in symmetry, and a structural transition in a hydride material might also be indistinguishable using XRD if the heavy atom sublattice does not re-order, as is the case for the $R3m$ to $Im\bar{3}m$ transition in H_3S .¹⁰ Resistance continues to decrease with lowering temperature before a sharp drop to zero resistance as the critical temperature is crossed. Such a difference in T_c to that of Snider *et al.*¹¹ could be expected, as their thermodynamic approach to a superconducting state begins from cooling in the recently confirmed $Im\bar{3}m$ phase emerging above 159 GPa¹² rather than the previously reported phase IV.¹¹

SC-XRD measurements on other crystals were conducted at HP-CAT with $\lambda = 0.34453 \text{ \AA}$. Conical diamonds with 80° apertures were used for greater completeness in SC-XRD. Fig 2 shows the P - V response of 8 C-S-H crystals from 3 separate runs, with all data on phase III/IV collected during Run X2. 2nd-order Birch-Murnaghan equations of state are fit to each crystal and phase (values in Table SI). We observe subtle systematic differences in V - P relations across the different crystals measured at the same thermodynamic conditions. The largest difference in V is 2.9% at 28.9(5) GPa in Run X2 between crystals C1 and C4. K_0 was found

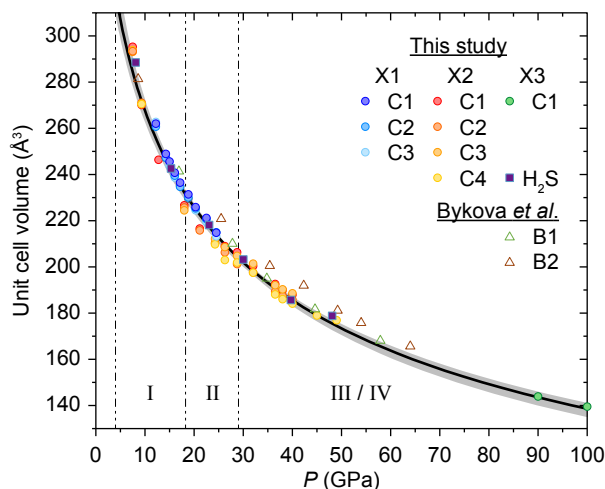


Fig. 2 *P-V* relations of C-S-H at 300 K compared with values from H₂S and Bykova *et al.*²⁶. A 2nd order Birch-Murnaghan equation of state was fit with initial volume $V_0 = 400.573 \text{ Å}^3$ and bulk modulus $K_0 = 11.028 \text{ GPa}$ (black line), and the gray area denotes uncertainty derived from high and low bands for Runs X1 and X2. Phase division for I (*I4/mcm*) → II (*C2/c*) → III/IV (*I4/mcm*) are taken from Snider *et al.*¹¹.

to range between 7.321 and 14.496 GPa for Runs X1 C3 and X2 C3. *V* trends for all of the C-S-H crystals measured are equal or lower than that of our own measurements on pure H₂S+H₂, which in turn is noticeably lower than that reported for C-S-H prepared from mixtures of molecular gases.²⁶ This, along with differences in the electronic response between crystals measured here and in Snider *et al.*¹¹, suggests a large variability in C-S-H stoichiometry generated by photochemistry under pressure.

Leading up to 18 GPa, SC-XRD measurements confirm phase I¹¹ as the Al₂Cu-type structure (*I4/mcm*) previously identified in CH₄-H₂ and H₂S-H₂ mixtures.^{26–28} The *I4/mcm* phase is inferred between 4 to 9 GPa as no change is observed by Raman spectroscopy. Due to insufficient C concentration or unique crystallographic placements, SC-XRD measurements are unable to resolve between C and S on the 8*h* Wyckoff positions, thus Fig 3a displays only H₂S units on the 8*h* sites. Applying the Bernal-Fowler "ice rules"²⁹ to determine the H positions within *I4/mcm* of the H₂S molecular units results in partially occupied 16*k* Wyckoff positions, and this constrains the H₂S molecular units to be planar within {002} as in Strobel *et al.*²⁸.

A CSP study on the H-S system identified a *P1* modification which mostly varies from the *I4/mcm* H positions owing to out-of-plane rotation of the molecular sub-units.⁹ Comparing several planar arrangements of the H atoms (keeping the lattice and S positions fixed at their experimental values) versus the arrangement of the *P1* structure with DFT and the vdW-DF2 functional shows a $\sim 0.44 \text{ eV}$ preference for a non-planar H arrangement.³⁰ This indicates C-S-H will have non-planar arrangements of H₂S molecular units to facilitate interactions between the shorter 3.30 Å inter-plane nearest neighbor S atoms. The magnitude of the enthalpic differences shows weak packing forces that could enable the molecular sub-units to behave as weakly constrained rotors within their respective molecular volume when thermalized.

Given the orientational preference in the interplane direction and the S-S nearest neighbor distances being within the van der Waals and H₂S dimer H-bonding distances,³¹ there is at least some weak H-bonding contributing to the cohesion of the lattice along with the primary van der Waals forces.

Above 18 GPa, C-S-H transforms into a *C2/c* phase (Fig 3b). This transition was observed in all crystals of Run X1 and in H₂S+H₂, but was not present in C1 and C4 of Run X2. The absence of *C2/c*-type C-S-H in some crystals is consistent with observations in Bykova *et al.*²⁶ and Goncharov *et al.*¹², where the phase is observed only in crystals with low C content, and further exemplifies the variation in stoichiometry in C-S-H formed by photochemistry. It is worth noting the similarities between the *C2/c* structure of C-S-H and previously documented structures of H-S. The *Cccm* H-S structure from Duan *et al.*⁹ is preferred by Pace *et al.*³² owing to its H-S-H network providing an additional distinct environment for molecular H₂ units, which is reflected in the Raman vibron. This and the *I222* structure reported by Strobel *et al.*²⁸ differ from the *C2/c* structure only in the orientation of H₂S sub-units and apparent directionality of the H bonding network. The *C2/c* phase resembles a monoclinically-distorted version of the *I4/mcm* phase where the [101] direction of the *C2/c* structure roughly corresponds to the [001] direction of the *I4/mcm* structure. In both cases, that direction resembles a 2-dimensional pore formed by S atoms interconnected by inter-plane H-bonding that encapsulates the H₂ molecules, and the views shown in Fig 3 are all oriented to look along this pore-like structure. The H positions determined by SC-XRD are reminiscent of the 9 GPa structural optimizations.

C-S-H transforms back into an *I4/mcm* structure around 29 GPa (Fig 3c) which persists to our highest measurements at 100 GPa. Our measured phase transitions by SC-XRD agree well with those reported in Raman studies.¹¹ The H positions of the H₂S units are again best modeled crystallographically within the constraint of the *I4/mcm* group to be in a planar configuration. However, DFT dictates that orientations with out-of-plane H positions are 5–7 eV more enthalpically favorable, and the lowest enthalpy configuration found here (structure in ESI, but like Fig 3d) shows a H-bonding network creating 2 dimensional channels along [001].

The previous reported transformation from phase III to IV around 45 GPa or metallization above 60 GPa are not distinguished by SC-XRD as the structural solution remains *I4/mcm* up to our highest measurement at 100 GPa. Optimizing the lowest enthalpy 50 GPa configuration using the lattice and S positions determined by SC-XRD at 90 GPa shows a H-bond symmetrization along [001] as in *Im $\bar{3}m$* H₃S (Fig 3d).¹⁰ Other configurations were evaluated confirming the structure with zig-zag H-bonding along [001] is the most enthalpically favorable at 90 GPa. This marks a transition from a double-well to a single-well potential for those H atoms, and is accompanied by a significant drop in the band gap (of the S and H only system) from 1.99 eV at 50 GPa to 0.25 eV at 90 GPa. Thus, the transition from phase III to phase IV is this transition from H-bonding to covalency which eventually drives metallization. It should be noted that the planar configurations considered at 50 and 90 GPa are metallic, so any H₂S molecules metastably trapped in planar orientations could drive

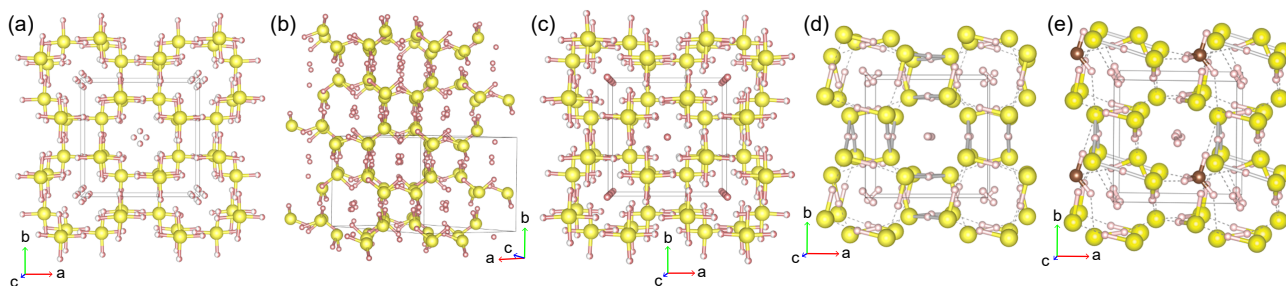


Fig. 3 SC-XRD determined structure at (a) 9 GPa $I4/mcm$ (b) 29 GPa $C2/c$ and (c) 50 GPa $I4/mcm$ C-S-H. (d) DFT derived structure at 90 GPa – bicolor cylinders represent bonds (≤ 1.43 Å), silver cylinders represent H atoms shared between two heavy atoms (1.43–1.53 Å), and dashed lines represent H bonds (1.53–2.0 Å). (e) Lowest enthalpy structure found here when substituting a CH_4 for an H_2S in the 90 GPa structure shown in (d). Yellow spheres represent S throughout, brown spheres C, and pink spheres H.

metallization sooner than the double-to-single well transition.

A prototypical carbonaceous model can be created by substituting one of the H_2S molecules of Fig. 3d with a CH_4 molecule. Optimizing the H positions of that model shows a disruption to the zig-zag S–H–S network along [001] in the vicinity of the CH_4 (structure in ESI), coupled with a reduction of metallicity compared to the S–H system. The lowest enthalpy structure found increases the band gap to 1.36 eV but does orient the CH_4 to form linkages reminiscent of those seen in $R3m$ CSH₇.²⁰ A higher enthalpy (structure in ESI) structure rotates the CH_4 such that the adjacent H_2S molecules are more like Fig 3d accompanied by a ~ 0.27 eV lower band gap. While a metallic modification of this model was not identified here, these results suggest that the turning points of the $R(T)$ curves in Fig. 1a arise from orientational ordering and H-bond symmetrization within the C-S-H sample.

In conclusion, new transport measurements on C-S-H with greater C content show a transition to a superconducting state with maximum T_c of 191 K at 91 GPa – significantly lower than previously observed. SC-XRD confirms a phase evolution of $I4/mcm$ to $C2/c$ to $I4/mcm$ in crystals with lower C content, while more carbonated crystals bypass the monoclinic phase. The absence of an measurable transition from phase III to IV seen in earlier Raman studies indicates that the transition is likely a re-ordering of the H which leaves the S sublattice unchanged, which is supported by DFT simulations. That greater C content inhibits the formation of monoclinic C-S-H, but also promotes a transition to a superconducting state at significantly lower pressures is worthy of further study, and a major challenge for the study of C-S-H is to ensure control of the product and controllable concentration of the constituent elements during the photo-induced reaction.

This work supported by the U.S. Department of Energy, Office of Basic Energy Sciences under Award Number DE-SC0020303. This research is funded in part by the Gordon and Betty Moore Foundations EPiQS Initiative, Grant GBMF10731 to AS and RPD. Portions of this work were performed at HPCAT (Sector 16), Advanced Photon Source (APS), Argonne National Laboratory. HPCAT operations are supported by DOE-NNSA Office of Experimental Sciences. The Advanced Photon Source is a U.S. Department of Energy (DOE) Office of Science User Facility operated for the DOE Office of Science by Argonne National Laboratory under Contract No. DE-AC02-06CH11357.

Conflicts of interest

There are no conflicts to declare.

Notes and references

- N. W. Ashcroft, *Phys. Rev. Lett.*, 2004, **92**, 187002.
- E. Wigner and H. B. Huntington, *J. Chem. Phys.*, 1935, **3**, 764–770.
- N. W. Ashcroft, *Phys. Rev. Lett.*, 1968, **21**, 1748–1749.
- C. F. Richardson and N. W. Ashcroft, *Phys. Rev. Lett.*, 1997, **78**, 118–121.
- C. J. Pickard, I. Errea and M. I. Erements, *Annu. Rev. Condens. Mater. Phys.*, 2020, **11**, 57–76.
- E. Snider, N. Dasenbrock-Gammon, R. McBride, X. Wang, N. Meyers, K. V. Lawler, E. Zurek, A. Salamat and R. P. Dias, *Phys. Rev. Lett.*, 2021, **126**, 117003.
- F. Belli, T. Novoa, J. Contreras-García and I. Errea, *Nature Commun.*, 2021, **12**, 5381.
- A. P. Drozdov, M. I. Erements, I. A. Troyan, V. Ksenofontov and S. I. Shylin, *Nature*, 2015, **525**, 73–76.
- D. Duan, Y. Liu, F. Tian, D. Li, X. Huang, Z. Zhao, H. Yu, B. Liu, W. Tian and T. Cui, *Sci. Rep.*, 2014, **4**, 6968.
- I. Errea, M. Calandra, C. J. Pickard, J. R. Nelson, R. J. Needs, Y. Li, H. Liu, Y. Zhang, Y. Ma and F. Mauri, *Nature*, 2016, **532**, 81–84.
- E. Snider, N. Dasenbrock-Gammon, R. McBride, M. Debesai, H. Vindana, K. Vencatasamy, K. Lawler, A. Salamat and R. Dias, *Nature*, 2020, **586**, 373–377.
- A. F. Goncharov, E. Bykova, M. Bykov, X. Zhang, Y. Wang, S. Chariton, V. B. Prakapenka and J. S. Smith, *J. Appl. Phys.*, 2022, **131**, 025902.
- W. Cui, T. Bi, J. Shi, Y. Li, H. Liu, E. Zurek and R. J. Hemley, *Phys. Rev. B*, 2020, **101**, 134504.
- Y. Sun, Y. Tian, B. Jiang, X. Li, H. Li, T. Itaka, X. Zhong and Y. Xie, *Phys. Rev. B*, 2020, **101**, 174102.
- Y. Ge, F. Zhang, R. P. Dias, R. J. Hemley and Y. Yao, *Materials Today Physics*, 2020, **15**, 100330.
- S. X. Hu, R. Paul, V. V. Karasiev and R. P. Dias, *Carbon-Doped Sulfur Hydrides as Room-Temperature Superconductors at 270 GPa*, 2020.
- T. Wang, M. Hirayama, T. Nomoto, T. Koretsune, R. Arita and J. A. Flores-Livas, *Phys. Rev. B*, 2021, **104**, 064510.
- X. Wang, T. Bi, K. P. Hilleke, A. Lamichhane, R. J. Hemley and E. Zurek, *A Little Bit of Carbon Can do a Lot for Superconductivity in H_3S* , 2021.
- D. R. Harshman and A. T. Fiory, *J. Appl. Phys.*, 2022, **131**, 015105.
- L. Novakovic, D. Sayre, D. Schacher, R. P. Dias, A. Salamat and K. V. Lawler, *Phys. Rev. B*, 2022, **105**, 024512.
- I. A. Troyan, D. V. Semenok, A. G. Kvashnin, A. V. Sadakov, O. A. Sobolevskiy, V. M. Pudalov, A. G. Ivanova, V. B. Prakapenka, E. Greenberg, A. G. Gavriluk, I. S. Lyubutin, V. V. Struzhkin, A. Bergara, I. Errea, R. Bianco, M. Calandra, F. Mauri, L. Monacelli, R. Akashi and A. R. Oganov, *Adv. Mater.*, 2021, **33**, 2006832.
- X. Zhang, Y. Zhao, F. Li and G. Yang, *Matter Radiat. at Extremes*, 2021, **6**, 068201.
- G. Shen, Y. Wang, A. Dewaele, C. Wu, D. E. Fratanduono, J. Eggert, S. Klotz, K. F. Dziubek, P. Loubeyre, O. V. Fatyanov, P. D. Asimov, T. Mashimo, R. M. M. Wentzcovitch and other members of the IPPS task group, *High Pressure Research*, 2020, **40**, 299–314.
- D. Smith, D. P. Shelton, P. B. Ellison and A. Salamat, *Rev. Sci. Instrum.*, 2018, **89**, 103902.
- M. Einaga, M. Sakata, T. Ishikawa, K. Shimizu, M. Erements, A. Drozdov, I. Troyan, N. Hirao and Y. Ohishi, *Nature Phys.*, 2016, **12**, 835–838.
- E. Bykova, M. Bykov, S. Chariton, V. B. Prakapenka, K. Glazyrin, A. Aslandukov, A. Aslandukova, G. Criniti, A. Kurnosov and A. F. Goncharov, *Phys. Rev. B*, 2021, **103**, L140105.
- M. S. Somayazulu, L. W. Finger, R. J. Hemley and H. K. Mao, *Science*, 1996, **271**, 1400–1402.
- T. A. Strobel, P. Ganesh, M. Somayazulu, P. R. C. Kent and R. J. Hemley, *Phys. Rev. Lett.*, 2011, **107**, 255503.
- J. D. Bernal and R. H. Fowler, *J. Chem. Phys.*, 1933, **1**, 515–548.
- K. Lee, E. D. Murray, L. Kong, B. I. Lundqvist and D. C. Langreth, *Phys. Rev. B*, 2010, **82**, 081101.
- A. Das, P. K. Mandal, F. J. Lovas, C. Medcraft, N. R. Walker and E. Arunan, *Angew. Chem., Int. Ed.*, 2018, **57**, 15199–15203.
- E. J. Pace, X.-D. Liu, P. Dalladay-Simpson, J. Binns, M. Peña Alvarez, J. P. Attfield, R. T. Howie and E. Gregoryanz, *Phys. Rev. B*, 2020, **101**, 174511.